

# Effects of Pressure Application Method on Transparency of Spark Plasma Sintered Alumina

Salvatore Grasso,<sup>‡,§</sup> Chunfeng Hu,<sup>§</sup> Giovanni Maizza,<sup>¶</sup> Byung-Nam Kim,<sup>§</sup> and Yoshio Sakka<sup>\*,†,‡,§</sup>

<sup>‡</sup>Graduate School of Pure and Applied Sciences, University of Tsukuba, Ibaraki 305-0047, Japan

<sup>§</sup>World Premier International Research Center Initiative (WPI Initiative) on Materials Nanoarchitectonics (MANA) and Nano Ceramics Center, National Institute for Materials Science (NIMS), Ibaraki 305-0047, Japan

<sup>¶</sup>Dipartimento di Scienza dei Materiali ed Ingegneria Chimica, Politecnico di Torino, I-10129 Torino, Italy

**Commercially available alumina powder was consolidated at 1150°C by spark plasma sintering at the heating rate of 100°C/min. The effects of the pressure application mode were examined with respect to microstructure, porosity, and transparency. A finite-element simulation was developed in order to understand the relationship between sample homogeneity and its temperature distribution. The effects of the temperature probing point on the microstructure were investigated. The application of two steps pressure was found effective to obtain homogeneously densified translucent alumina samples at high heating rate.**

## I. Introduction

As reported in literature, translucent alumina with an average grain sizes of 0.5–0.6  $\mu\text{m}$  and densities of about 99.8% has been traditionally used as structural ceramic because of the very high hardness (20–21  $\text{GPa}^{1,2}$ ) and elevated three-point bending strength (750–900  $\text{MPa}^1$ ). The excellent mechanical properties combined with in line transmittance exceeding 50 % make this material particularly suitable for the production of ceramics for lamp envelopes and other structural applications. Traditionally translucent alumina is manufactured by hot isostatic pressing (HIP), however recently, spark plasma sintering (SPS) has been considered as an alternative method to obtain nearly full dense fine-grained translucent alumina.<sup>3–7</sup> Owing to the advantage of rapid heating, the alumina ceramics obtained by SPS have a grain size and density comparable to those of HIPed ones.<sup>8</sup> Several investigation focused on the consolidation of transparent alumina by SPS. Kim *et al.*<sup>3,5</sup> reported that in the case of slow heating of 2°C/min rate was possible to obtain transparency as high as 47%, conversely, in the case of 100°C/min the transmittance was as low as 0.2%. The latter results has been confirmed in terms of porosity by Aman and colleagues (see fig. 3 of Aman *et al.*<sup>7</sup>).

Most of the investigation reported that is rather difficult to obtain translucent alumina by SPS at the heating rate of 100°C/min.<sup>3,5,7</sup> At present, the effect of the heating rate on the transparency of SPSed alumina has been not yet fully elucidated. However, from a technological point of view, sintering at high heating rate is strongly desired in order to: (i) increase the productivity, (ii) decrease the specific energy consumption of the consolidation process.

For example, Kim and colleagues in order to achieve a transparency of 47% used a sintering cycle of about 6 h (i.e., 2°C/min), such long processing time strongly limits the production rate. Furthermore, the SPS is well known as a rapid sintering technology, consequently the use of low heating rate would limit its intrinsic advantage.<sup>9</sup> The SPS processes are energetically efficient because they can use two-thirds to four-fifths of the energy needed by conventional HP.<sup>10</sup> On the other hand, when slow heating rate are used, the heat is rapidly extracted by the cooling system and radiated from the graphite surfaces to the inner wall of the SPS furnace. The reduction of the heating and dwelling time can enormously contribute to reduce the heat dissipated by the cooling system.

The present work is divided in two parts. In the first part, the effect of the temperature probing point with respect to the microstructure and grain growth (Section III(1)) are analyzed. In the second part, a combined experimental numerical simulation is developed in order to understand the sintering mechanism of alumina processed at high heating rate (Section III(2)). The effects of the pressure application mode along with experimental and numerical analysis are discussed.

## II. Experimental Procedure

Commercially available  $\alpha\text{-Al}_2\text{O}_3$  powder (TM-DAR, Taimai Chemicals Co. Ltd., Tokyo, Japan), with a purity of 99.99% and an average particle size of 0.2  $\mu\text{m}$ , was used in this study. The as-received powder was directly poured into a graphite die without any special treatment or additives. The inner and outer diameters of the graphite die were 30 and 70 mm respectively, the height of the die was 60 mm. The height and the diameter of the punches were both 30 mm. The two pairs of graphite spacers ( $\varnothing 80$  height 40 mm and  $\varnothing 120$  height 20 mm) were pushed between the water-cooled rams made up of steel ( $\varnothing 120$  height 20 mm). The temperature was accurately measured by two pyrometers,<sup>11</sup> the side pyrometer was focused on the die surface (hereinafter, side pyrometer). The top pyrometer was focused on nontrough hole ( $\varnothing 9$  mm) inside the punch (at the center of the punch mid thickness). A drawing showing the temperature probing point is given below in Fig. 5. The double pyrometers configuration was at first calibrated. The SPS machine was operated in temperature control mode, and the temperature was measured at the same time by the top and side pyrometers. In order to reduce the heat loss by radiation a graphite felt (1 cm thick) was used.

In all experiments an identical heating cycle was used: the temperature was raised up to 700°C in 10 min consequently the heating rate up to 1150°C was 100°C/min. The dwelling times at 1150°C were 30 and 60 min. The pressure was applied in two ways, in the first case a *constant pressure* of 80 MPa was applied for the entire duration of the sintering process (hereinafter,

J. Blendell—contributing editor

Manuscript No. 27891. Received April 22, 2010; approved October 29, 2010.

This work was supported by World Premier International Research Center Initiative (WPI Initiative), MEXT, Japan.

\*Member, The American Ceramic Society.

†Author to whom correspondence should be addressed. e-mail: sakka.yoshio@nims.go.jp

constant pressure). In the second case, the initial pressure of 35 MPa was applied, subsequently the pressure was increased in 3 min after the beginning of dwelling time (hereinafter, *two steps pressure*). Heating was conducted using a sequence consisting of 12 DC pulses (40.8 ms) followed by power off for 6.8 ms. Finally, we obtained a sintered disk with a diameter of 30 mm and a thickness of 3 mm. The entire disk body was machined to a disk of 30 mm diameter with a thickness of 1 mm, and mirror-polished carefully on both sides using diamond slurry. The final thickness of the sample was about 0.8 mm. The in-line transmission was measured in the wavelength range from 0.24 to 1.6  $\mu\text{m}$  using a double-beam spectrophotometer (SolidSpec-3700DUV, Shimadzu, Kyoto, Japan). The distance between the sample and the detector was about 55 cm.

The fracture surfaces and thermally etched surfaces (950°C for 1 h) were observed by means of a scanning electron microscope (SEM) (JSM-7100, JEOL, Tokyo, Japan). The porosity was measured on the SEM images of the polished and thermally etched surfaces taken at a magnification of 10 000 times. We did not measure the absolute density because the conventional techniques such as the Archimedes method are insensitive to extremely low porosity.

The grain size, observed on the SEM images of the polished and thermally etched surfaces, was calculated by obtaining the average cross-section area per grain and assuming spherical grains. The measured grain size is an apparent one, so that it was multiplied by 1.225 to determine the true grain size.<sup>8</sup>

A finite-element model was developed to predict the temperature distribution of the alumina sample. The model permitted to understand the relationship between temperature distribution and densification inside the alumina samples. The model used an integrated experimental/numerical methodology, which simultaneously permitted the developed SPS model to be reliably tested against experiments. The SPS model coupled electrothermal and displacement fields; the contact multiphysics at the sliding punch/die interface was modeled during powder sintering using a moving mesh/moving boundary technique. The SPS model used here assumes uniform displacement and stress within the sample. The displacement history is taken from experiments and it prescribes the average density of the sample. Coupling between electrothermal field and displacement is made through the evolving average density. The friction between punch and die is not taken into account in the model. Model details can be found in Maizza *et al.*<sup>12,13</sup> The thermal conductivity of the pressed alumina powders assumed in the FEM calculations was experimentally measured by a Xenon flash apparatus (LFA447 Nanoflash, Netzsch, Selb, Germany).

### III. Result and Discussions

#### (1) Effect of the Temperature Probing Point

Usually SPS machine are operated in temperature control mode. The temperature is measured at a probing point while the voltage/current is continually adjusted to fulfill the desired heating/cooling cycle. Especially in the case of high heating rate is important to choose the probing point in order to accurately heat the powder up to the desired sintering temperature at programmed heating rate without overheating.

Figure 1 shows the voltage and temperature profiles in the case of alumina samples sintered by controlling the temperature from (a) the top and (b) side pyrometer. In the case of control from the top, the top temperature did not exceeded 1150°C. As shown in Fig. 1(a), during the heating at temperature above 1000°C, the temperature difference  $\Delta T$ , between top and side pyrometer was around +43°C. The temperature difference  $\Delta T$  during the dwelling time decreased to +5°C.

On the contrary to the top pyrometer control, it was not possible to accurately control the temperature in the case the side pyrometer (Fig. 2(b)). At the end of the heating (e.g., before the dwelling), the temperatures measured at the top and side pyrometer were 1230° and 1190°C, respectively. Such overheating was attributed to the thermal gradient  $\Delta T$  and to the temperature oscillation respect to the programmed temperature cycle (i.e., 1150°C). The voltage rapidly fluctuated during the temperature oscillations due to the instability of the temperature control.

By controlling the temperature from top, it was possible to adjust the voltage in order to fulfill the programmed temperature cycle. In fact in the case of top pyrometer, unlike the side one, no significant overheating was measured. The temperature was directly measured nearby the heating source of the punch-die assembly and consequently the voltage could be properly adjusted by the SPS machine control.

As shown in Fig. 1, the probing point affected the stability of automatic the SPS control voltage/current in terms of temperature overheating and temperature oscillation respect to the programmed temperature cycle. Depending on the temperature probing point, top or side, the average grain sizes observed in the center of the sample were 0.47 and 0.83  $\mu\text{m}$ , respectively. In the case of temperature controlled from the side (Fig. 1(b)), the overheating enhanced severe grain growth (Fig. 2(b)), on the contrary, in the case of top pyrometer (Fig. 1(a)) the accurate temperature control limited the grain growth (Fig. 2(a)). In the case of high heating rate SPS (i.e., 100°C/min), in order to obtain finer microstructure and more accurate control of the

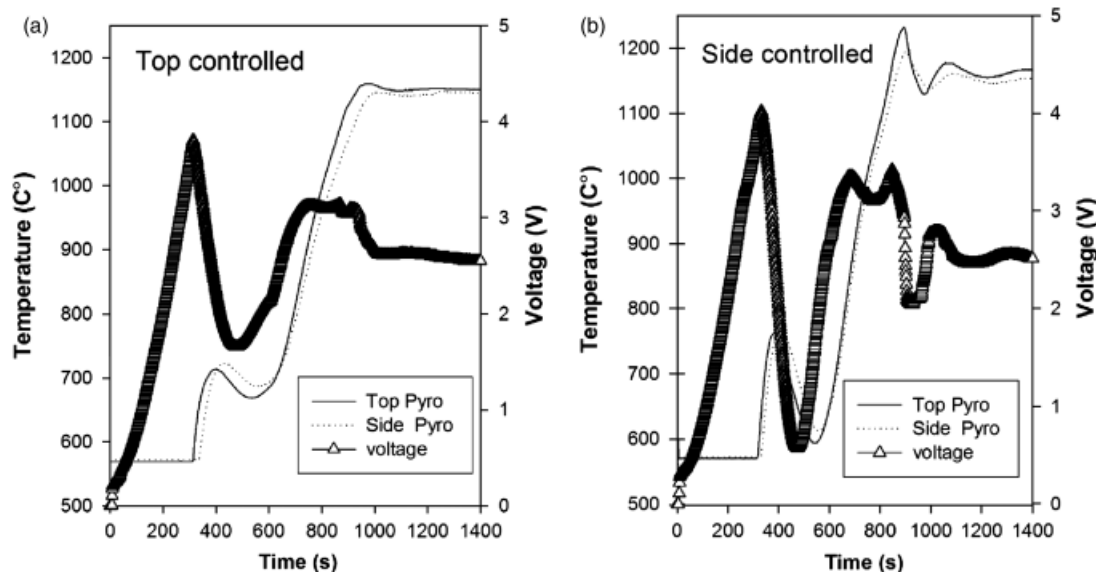
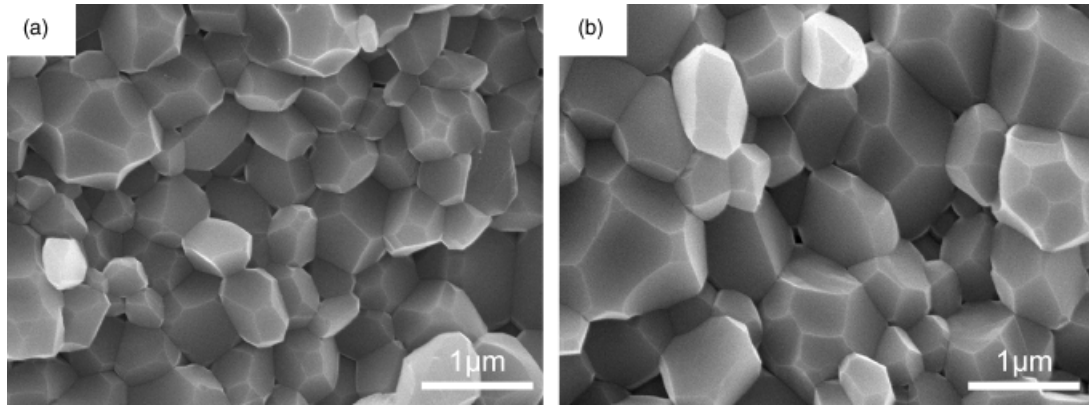


Fig. 1. Effect of the temperature probing point on the voltage and temperature profiles as function of time. SPS apparatus was controlled (a) from the top pyrometer (b) from the side pyrometer.



**Fig. 2.** FESEM of intragranular fracture surface of alumina sample sintered at 1150°C for 30 min heated at 100°C/min under *constant pressure* of 80 MPa. The temperature was controlled from the top (a) and from the side (b) pyrometers.

sintering temperature, the machine should be operated by controlling the temperature from the top pyrometer.

### (2) Combined Experimental and Modeling Analysis of the Pressure Application Mode

Figure 3 shows a photograph of sintered alumina samples with a thickness of about 0.8 mm on top of the text. The samples A–C were sintered at 1150°C at a heating rate of 100°C/min, the SPS machine was controlled by the top pyrometer. The sample A was sintered under 80 MPa *constant pressure* for 30 min. As shown in the inset Figure 3 of sample A, the border of the sample (1.5 mm width) hereinafter defined as  $A^{\text{border}}$ , is translucent while the inner part  $A^{\text{center}}$  is opaque. In the case of samples B and C the pressure was raised from 35 to 80 MPa 3 min after the beginning of the dwelling time (*two steps pressure*). The holding time at the sintering temperature were 30 and 60 min, respectively. The transmittance measured at the center of the samples A–C along with the grain size and residual porosity are given in Table I. The grain size of sample B is shown in Fig. 4. It was not possible to measure the transmittance of sample  $A^{\text{border}}$  because the translucent area was not big enough to permit the measurement.

Despite the identical powder, sintering temperature, heating rate and holding time, the transmittance and the porosity of samples prepared by SPS are quite different depending on the pressure application method. By comparing samples A and B the in-line transmittance increased from 0.3% to 15.7%. The

reason of such significant dissimilarity of the transmittance can be attributed to the residual porosity.<sup>14</sup> In fact in the case of sample  $A^{\text{center}}$  the porosity was 1.26% which completely deteriorated the transmittance, instead in the case of sample B the porosity was 0.20%.

The FEM simulation, developed in Maizza *et al.*,<sup>12,13</sup> calculated the temperature distribution inside the sample and permitted to understand the densification mechanism in the case of *constant pressure* application. Figure 5 shows the temperature distribution inside (a) the punch-die sample assembly and (b) sample calculated before the holding at 1150°C (i.e., at the end of the heating cycle). Because the alumina behaves as electric insulator, the Joule heating due to the current flowing inside the sample is substantially negligible.<sup>15</sup> Owing to the low thermal conductivity of the pressed alumina powders (0.6 W/m·K)<sup>16,17</sup> and the high heating rate (100°C/min), the heat was slowly conducted from the punch-die assembly through pressed alumina powder and a significant thermal gradient of 42°C was generated inside the sample (Fig. 5(b)).

The densification mechanism in the case of *constant pressure* can be schematized as follows:

(1) The sample border was 42°C hotter (Fig. 5(b)) than the center due to the high heating rate and poor thermal conductivity of the pressed alumina powders. The latter promoted the densification of the hotter region sample (sample  $A^{\text{border}}$ ).

(2) During the holding at 1150°C, the sample  $A^{\text{border}}$  and  $A^{\text{center}}$  densified up to 99.92% and 98.74%, respectively (see

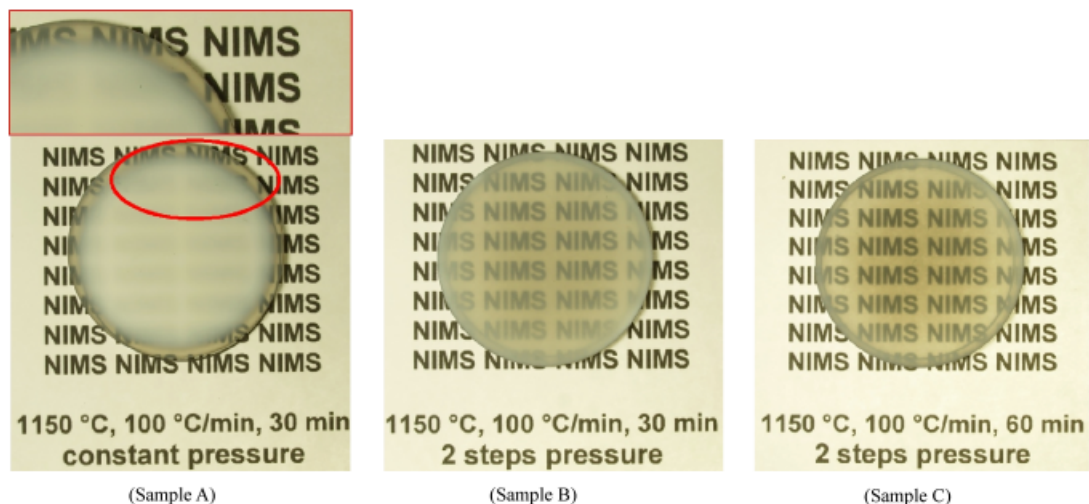


**Fig. 3.** Photograph of alumina ceramics disks sintered by SPS at 1150°C with a heating rate of 100 C/min. The sample shown in figure (a) was sintered for 30 min under 80 MPa *constant pressure*. The sample (b) and (c) were sintered with pressure *two steps pressure* application for 30 and 60 min. The samples are 3 cm in diameter and are on top of the text.

**Table I. Sintering Conditions (Sintering Temperature, Holding Time, Pressure Application Method), Grain Size, Residual Porosity, and in Line Transmittance (Measured at a Wavelength of 645 nm) of the Sintered Samples**

Sample name	Sintering conditions	Grain size ( $\mu\text{m}$ )	Porosity (%)	In line transmittance (%)
Sample A <sup>center</sup>	1150 C, 30 min, constant pressure	0.47	1.26	0.33
Sample A <sup>border</sup>		0.39	0.08	—
Sample B	1150 C, 30 min, 2 steps pressure	0.41	0.20	15.7
Sample C	1150 C, 60 min, 2 steps pressure	0.47	0.14	19.8

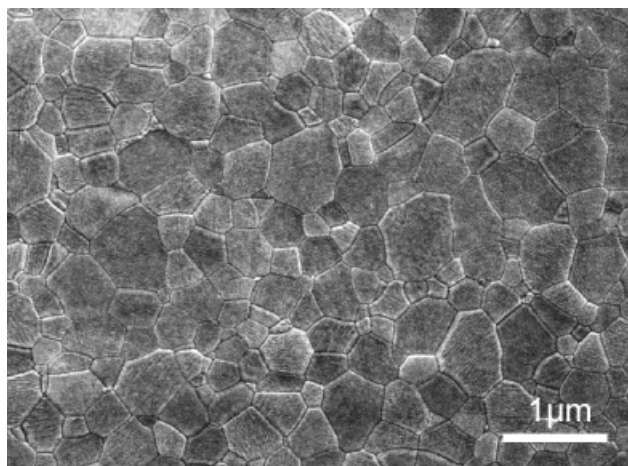
**Fig. 4.** Microstructures of the sample B alumina sintered for 30 min at 1150°C with heating rate of 1150°C.

Table I). The highly dense sample A<sup>border</sup> prevented the further shrinkage of the powder along the pressing direction.

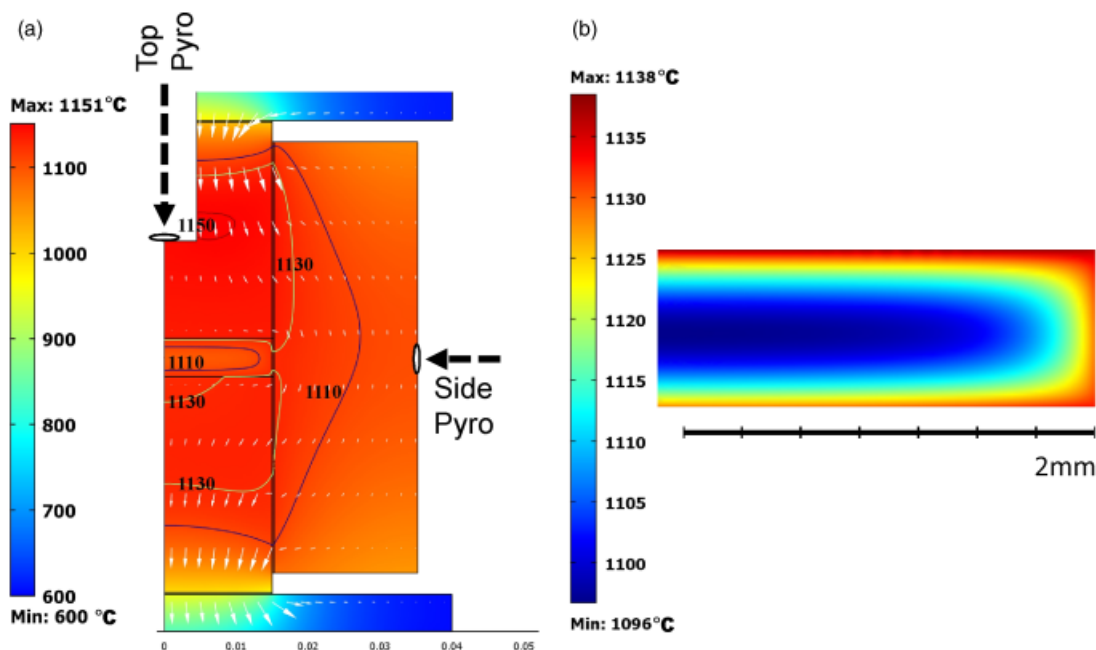
Similarly to present investigation, Wang *et al.*<sup>18,19</sup> reported that the temperature gradient inside the sample resulted in differential densification which corresponded to a gradual decrease of hardness from the border to center of the alumina samples.

In the case of the *constant pressure*, the sample A<sup>border</sup>, due to the higher temperature, densified at a higher rate than the sample A<sup>center</sup>, consequently more dense sample border limited the punch shrinkage and consequently inhibited the center from

densifying fully. McWilliams and Zavaliangos<sup>20</sup> investigated developed a FEM model which coupled the thermal-electric and free (i.e., the compact is not constrained in a die or under pressure) sintering phenomena. Similarly as in the present study, the thermal gradient inside the sample generated non homogeneously densified samples.<sup>20</sup>

On the contrary to *constant pressure*, in the case of *two steps pressure* (sample B and C Fig. 3) it was possible to obtain translucent alumina ceramics with grain size about 0.4  $\mu\text{m}$  and final density >99.8%. The initial pressure of 35 MPa was insufficient to achieve high level of densification. After 3 min the beginning of the dwelling time, the thermal gradient inside the sample decreased down to 5°C (as given by FEM simulation) and the pressure elevation up to 80 MPa permitted to obtain homogeneously densified translucent alumina as shown in Fig. 3. In the case of samples B and C, by extending the holding time from 30 to 60 min the porosity decreased from 0.2 to 0.14 while the in line transmittance (for wavelength of 645 nm) increased from 15.6% to 19.8%. No significant difference in the microstructure along the sample radius was observed. The pressure elevation 3 min after the beginning of the dwelling permitted lower the thermal gradient inside the sample (e.g., 5°C as given by FEM results) and offered an effective means to obtain translucent alumina at high heating rate.

In the case of high heating rate SPS, *two steps pressure* and *constant pressure* led to translucent and opaque samples, respectively. Indeed, the samples obtained by *two steps pressure* were more dense and more homogeneously densified than the one obtained by *constant pressure*. The developed SPS model, together with the *two-step pressure* method, is an aiding tool to predict the temperature distribution inside the sample and to elucidate the mechanism for obtaining homogeneously densified translucent alumina ceramics.

**Fig. 5.** Temperature distribution inside (a) the punch-die sample assembly and (b) sample calculated before the dwelling time (i.e., at the end of the heating cycle). Arrows plot shows the current distribution.

#### IV. Conclusion

In addition to previously reported investigations it was possible to increase the transmittance of translucent alumina prepared by high heating-rate SPS when the maximum pressure was applied during a later stage of the sintering process. It is shown that the control from the top pyrometer prevented powder overheating and consequently the grain growth. The pressure application method was crucial to obtain homogeneously densified translucent sample.

The application of *constant pressure* led to non-homogeneously densified sample due to the significant thermal gradient generated during the heating. The border of the sample was highly densified (i.e., porosity 0.08%) while the center was porous (i.e., porosity 1.26%).

The *two-step pressure method* was effective to obtain homogeneously densified translucent alumina ceramics with grain size of about 0.4  $\mu\text{m}$  and porosity below 0.2%. The initial pressure of 35 MPa was insufficient to achieve high level of densification. After 3 min the beginning of the dwelling time, the thermal gradient inside the sample decreased down to 5°C, consequently the pressure elevation up to 80 MPa permitted to obtain homogeneously densified translucent samples.

The *two-step pressure* method enabled a significant improvement of the degree of in line-transmittance of high-heating rate SPSed alumina. However, in the case of alumina sintered under pressure not exceeding 80 MPa, it is another confirmation of previously published results of this working group that high-rate SPS does not achieve a complete elimination of pores on the level requested for high transparency.

#### Acknowledgments

The authors are grateful to Dr. Toshiyuki Nishimura for providing the measurement of the thermal conductivity of the Alumina used in the present study.

#### References

- <sup>1</sup>A. Krell, P. Blank, H. Ma, and T. Hutzler, "Transparent Sintered Corundum with High Hardness and Strength," *J. Am. Ceram. Soc.*, **86**, 12–8 (2003).
- <sup>2</sup>A. Krell and S. Schädlich, "Nanoindentation Hardness of Submicrometer Alumina Ceramics," *Mater. Sci. Eng. A*, **307**, 172–81 (2001).

- <sup>3</sup>B. Kim, K. Hiraga, K. Morita, and H. Yoshida, "Effects of Heating Rate on Microstructure and Transparency of Spark-Plasma-Sintered Alumina," *J. Eur. Ceram. Soc.*, **29**, 323–7 (2009).

- <sup>4</sup>B. Kim, K. Hiraga, K. Morita, and H. Yoshida, "Spark Plasma Sintering of Transparent Alumina," *Scr. Mater.*, **57**, 607–10 (2007).

- <sup>5</sup>B. Kim, K. Hiraga, K. Morita, H. Yoshida, T. Miyazaki, and Y. Kagawa, "Microstructure and Optical Properties of Transparent Alumina," *Acta Mater.*, **57**, 1319–26 (2009).

- <sup>6</sup>Y. Aman, V. Garnie, and E. Djurado, "Influence of Green State Processes on the Sintering Behaviour and the Subsequent Optical Properties of Spark Plasma Sintered Alumina," *J. Eur. Ceram. Soc.*, **29**, 3363–70 (2009).

- <sup>7</sup>Y. Aman, V. Garnier, and E. Djurado, "A Screening Design Approach for the Understanding of Spark Plasma Sintering Parameters: A Case of Translucent Polycrystalline Undoped Alumina," *Int. J. Appl. Ceram. Technol.*, **7**, 574–86 (2010).

- <sup>8</sup>R. Apetz and M. P. B. Bruggen, "Transparent Alumina: A Light-Scattering Model," *J. Am. Ceram. Soc.*, **86**, 480–6 (2003).

- <sup>9</sup>S. Grasso, Y. Sakka, and G. Maizza, "Electric Current Activated/Assisted Sintering (ECAS): A Review of Patents 1906–2008," *Sci. Technol. Adv. Mater.*, **10**, 053001 (2009).

- <sup>10</sup>M. Tokita, "Large-Size Functionally Graded Materials Fabricated by Spark Plasma Sintering (SPS) method," *Mater. Sci. Forum*, **39**, 423–5 (2003).

- <sup>11</sup>K. Vanmeensel, A. Laptev, J. Hennicke, J. Vleugels, and O. Van der Biest, "Modelling of the Temperature Distribution during Field Assisted Sintering," *Acta Mater.*, **53**, 4379–88 (2005).

- <sup>12</sup>G. Maizza, S. Grasso, Y. Sakka, T. Noda, and O. Ohashi, "Relation between Microstructure, Properties and Spark Plasma Sintering (SPS) Parameters of Pure Ultrafine WC Powder," *Sci. Technol. Adv. Mater.*, **8**, 644–54 (2007).

- <sup>13</sup>G. Maizza, S. Grasso, and Y. Sakka, "Moving Finite-Element Mesh Model for Aiding Spark Plasma Sintering in Current Control Mode of Pure Ultrafine WC Powder," *J. Mater. Sci.*, **44**, 1219–36 (2009).

- <sup>14</sup>S. Grasso, B. Kim, C. Hu, G. Maizza, and Y. Sakka, "Highly Transparent Pure Alumina Fabricated by High-Pressure Spark Plasma Sintering," *J. Am. Ceram. Soc.*, **93**, 2460–2 (2010).

- <sup>15</sup>H. Tomino, H. Wantanabe, and Y. Kondo, "Electric Current Path and Temperature Distribution for Spark Sintering," *J. Jpn. Soc. Powder Powder Metall.*, **44**, 974–9 (1997).

- <sup>16</sup>L. Braginsky, V. Shklover, H. Hofmann, and P. Bowen, "High-Temperature Thermal Conductivity of Porous  $\text{Al}_2\text{O}_3$  Nanostructures," *Phys. Rev. B*, **70**, 134201 (2004).

- <sup>17</sup>W. N. dos Santos, "Effect of Moisture and Porosity on the Thermal Properties of a Conventional Refractory Concrete," *J. Eur. Ceram. Soc.*, **23**, 745–55 (2003).

- <sup>18</sup>S. W. Wang, L. D. Chen, T. Hirai, and Y. S. Kang, "Microstructure Inhomogeneity in  $\text{Al}_2\text{O}_3$  Sintered Bodies Formed During the Plasma-Activated Sintering Process," *J. of Mat. Sci. Lett.*, **18**, 1119–21 (1999).

- <sup>19</sup>S. W. Wang, L. D. Chen, and T. Hirai, "Densification of  $\text{Al}_2\text{O}_3$  Powder using Spark Plasma Sintering," *J. Mater. Res.*, **15**, 982–7 (2000).

- <sup>20</sup>B. McWilliams and A. Zavaliangos, "Multi-Phenomena Simulation of Electric Field Assisted Sintering," *J. Mater. Sci.*, **43**, 5031–5 (2008). □